

Pulse compression and multimegawatt optical solitons in hollow photonic-crystal fibers

A. D. Bessonov and A. M. Zheltikov*

Physics Department, International Laser Center, M. V. Lomonosov Moscow State University, Vorob'evy gory, Moscow 119992, Russia

(Received 26 December 2005; published 19 June 2006)

Solitonic phenomena in hollow photonic-crystal fibers are shown to offer new solutions for the control, transmission, and spectral-temporal transformation of ultrashort high-power laser pulses. With the initial parameters of laser radiation accurately matched with fiber dispersion and nonlinearity, submicrojoule laser pulses are shown to exhibit a self-compression and soliton dynamics in the regime of anomalous dispersion. Regimes of solitonic pulse evolution giving rise to few-cycle field waveforms are demonstrated. Based on simple arguments of soliton theory, we derive semiempirical relations providing interesting insights into the minimum pulse width of the laser field in a hollow photonic-crystal fiber as a function of the input laser energy.

DOI: [10.1103/PhysRevE.73.066618](https://doi.org/10.1103/PhysRevE.73.066618)

PACS number(s): 42.65.Wi

I. INTRODUCTION

Hollow-core photonic-crystal fibers (PCFs) [1,2] are optical waveguides of a novel type, which offer new interesting options for high-field physics and nonlinear optics. Diffraction-related radiation losses typical of hollow waveguides [3] can be substantially reduced for hollow PCFs relative to standard, solid-cladding hollow fibers [4,5] due to the high reflectivity of a periodic PCF cladding within photonic band gaps (PBGs) [1,2,6]. This enables transmission of high-intensity laser pulses through a hollow fiber core in isolated guided modes with typical transverse sizes of 10–20 μm . Due to this unique property, hollow PCFs can substantially enhance nonlinear-optical processes, demonstrating an outstanding performance in high-field nonlinear optics [7]. These waveguides have been recently demonstrated to radically enhance stimulated Raman scattering [8,9], four-wave mixing [10], coherent anti-Stokes Raman scattering [11], and self-phase modulation [12]. The spatial self-action of intense ultrashort laser pulses gives rise to interesting waveguiding regimes in hollow PCFs below the beam blowup threshold [13].

Air-guided modes in hollow PCFs can support megawatt optical solitons [14], allowing soliton pulse compression [15] and femtosecond soliton pulse delivery over large distances [16], as well as transportation of high-energy laser pulses for technological [17,18] and biomedical [19] applications. An all-fiber chirped-pulse amplification system based on compression in air-guiding photonic band-gap fiber has been demonstrated by Limpert *et al.* [20]. Recently, de Matos *et al.* [21] have shown that hollow-core PCFs allow the creation of all-fiber pulse compressors for high-peak-power pulses within a broad range of wavelengths. Highly birefringent hollow-core PCFs [22] have been used by Lim *et al.* [23] to simultaneously control polarization and support stretched-pulse operation in mode-locked ytterbium fiber lasers. All these results indicate the key role of PCFs in the development of the new all-fiber-format advanced ultrashort-pulse laser sources.

In this work, we show that the recently discovered solitonic regimes of pulse propagation in hollow PCFs [14–16]

offer new solutions for the control, transmission, as well as temporal and spectral transformation of ultrashort high-power laser pulses. We analyze self-compression and soliton formation scenarios of high-power laser pulse evolution in hollow PCFs with several typical profiles of group-velocity dispersion (GVD). Regimes of solitonic pulse evolution giving rise to few-cycle field waveforms will be demonstrated. Based on simple arguments of soliton theory, we derive semiempirical relations providing interesting insights into the minimum pulse width of the laser field in a hollow PCF as a function of the input laser energy.

II. GENERIC EQUATIONS AND NUMERICAL PROCEDURE

The key message of this work is that hollow PCFs allow formation of few-cycle field waveforms. We therefore have to abandon the slowly varying envelope approximation (SVEA), which cannot adequately describe the evolution of such short pulses and/or transformations of broadband spectra resulting from the evolution of ultrashort pulses in PCFs. The finite-difference time-domain (FDTD) technique provides a means for numerical solution of Maxwell equations for few-cycle and even subcycle field waveforms. However, in the case of large propagation lengths, typical of optical fibers, FDTD technique typically becomes impractical as it requires too much computational effort.

To analyze the self-compression and soliton dynamics of high-power laser pulses in hollow PCFs, we employ here an approach based on a numerical solution of the first-order non-SVEA unidirectional propagation equation for the Fourier transform of the field amplitude in waveguide modes of an optical fiber. The basic equation used in our treatment is similar to the equation derived earlier by Husakov and Herrmann for the evolution of laser pulses in the process of supercontinuum generation in PCFs [24]. This equation does not involve a Taylor-series approximation of the dispersion of the medium, but allows the exact dispersion profile of guided modes to be included in the analysis.

We start our treatment with the wave equation for the Fourier transform of the electric field, $\mathbf{E}=\mathbf{E}(\mathbf{r},\omega)=\text{FT}\{\mathbf{E}(\mathbf{r},t)\}$,

*Electronic address: zheltikov@phys.msu.ru

$$\nabla \times \nabla \times \mathbf{E} = k^2 \mathbf{E} + \mu_0 \omega^2 \mathbf{P}, \quad (1)$$

where $k = \omega/c$, ω is the radiation frequency, c is the speed of light, and \mathbf{P} is the polarization of the medium.

To include nonlinearity of the medium, we represent polarization \mathbf{P} as a sum of linear, \mathbf{P}_l , and nonlinear, \mathbf{P}_{nl} , parts,

$$\mathbf{P} = \mathbf{P}_l + \mathbf{P}_{nl}. \quad (2)$$

Substituting Eq. (2) into Eq. (1), we arrive at

$$\begin{aligned} (\Delta_{\perp} + k^2 n^2) \mathbf{E}(\mathbf{r}, \omega) + \nabla_{\perp} [\nabla_{\perp} \ln(n^2) \cdot \mathbf{E}(\mathbf{r}, \omega)] + \frac{\partial^2 \mathbf{E}(\mathbf{r}, \omega)}{\partial z^2} \\ + \mu_0 \omega^2 \mathbf{P}_{nl}(\mathbf{r}, \omega) = 0, \end{aligned} \quad (3)$$

where $n \equiv n(r, \omega)$ is the refractive index, Δ_{\perp} and ∇_{\perp} are the transverse parts of the Laplacian and gradient operators in the xy plane, and the nonlinear polarization appearing in the last term on the left-hand side is the Fourier transform of the time-domain nonlinear polarization of the medium.

We now assume that the field propagates along the z axis in an optical fiber and represent the electric field as

$$\mathbf{E}(\mathbf{r}, \omega) = E(z, \omega) \mathbf{E}(x, y, \omega), \quad (4)$$

where x and y are the transverse coordinates and $\mathbf{E}(x, y, \omega)$ is the Fourier transform of the field amplitude in the eigenmode of the fiber,

$$\mathbf{E}(\mathbf{r}, \omega) = \mathbf{E}(x, y, \omega) e^{i\beta z}, \quad (5)$$

with β being the propagation constant. The function $\mathbf{E}(x, y, \omega)$ and the parameter β are, respectively, the eigenfunction and the eigenvalue of the dispersion equation,

$$\begin{aligned} (\Delta_{\perp} + k^2 n^2) \mathbf{E}(x, y, \omega) + \nabla_{\perp} [\nabla_{\perp} \ln(n^2) \cdot \mathbf{E}(x, y, \omega)] \\ = \beta^2(\omega) \mathbf{E}(x, y, \omega). \end{aligned} \quad (6)$$

Using Eqs. (4) and (6) and neglecting spatial self-action effects, we rewrite Eq. (3) as

$$\frac{\partial^2 \mathbf{E}(\mathbf{r}, \omega)}{\partial z^2} + \beta^2 \mathbf{E}(\mathbf{r}, \omega) + \mu_0 \omega^2 \mathbf{P}_{nl}(\mathbf{r}, \omega) = 0. \quad (7)$$

Introducing

$$\beta_{nl}^2(z, \omega) = \beta^2(\omega) + \mu_0 \omega^2 B_{nl}(z, \omega), \quad (8)$$

where

$$B_{nl}(z, \omega) \mathbf{E}(r, \omega) = \mathbf{P}_{nl}(r, \omega), \quad (9)$$

we derive

$$\frac{\partial^2 \mathbf{E}(\mathbf{r}, \omega)}{\partial z^2} + \beta_{nl}^2(z, \omega) \mathbf{E}(\mathbf{r}, \omega) = 0. \quad (10)$$

We now express the operator on the left-hand side of Eq. (10) as

$$\frac{\partial^2}{\partial z^2} + \beta_{nl}^2 \approx \left(\frac{\partial}{\partial z} - i\beta_{nl} \right) \left(\frac{\partial}{\partial z} + i\beta_{nl} \right) \quad (11)$$

and neglect the reflected wave. In this approximation, Eq. (7) is reduced to

$$\frac{\partial \mathbf{E}(\mathbf{r}, \omega)}{\partial z} = i\beta_{nl}(z, \omega) \mathbf{E}(\mathbf{r}, \omega). \quad (12)$$

Assuming that the nonlinear part of the propagation constant β_{nl} is small as compared with its linear part, we represent this constant as a Taylor-series expansion,

$$\beta_{nl}(z, \omega) \approx \beta(\omega) + \frac{\mu_0 \omega^2}{2\beta(\omega)} B_{nl}, \quad (13)$$

and rewrite Eq. (12) as

$$\frac{\partial \mathbf{E}(\mathbf{r}, \omega)}{\partial z} = i\beta(\omega) \mathbf{E}(\mathbf{r}, \omega) + i \frac{\mu_0 \omega^2}{2\beta(\omega)} \mathbf{P}_{nl}(\mathbf{r}, \omega). \quad (14)$$

Introducing the retarded time $\eta = t - z/u$, where u is the group velocity, we derive

$$\frac{\partial \mathbf{E}(\mathbf{r}, \omega)}{\partial z} = i \left(\beta(\omega) - \frac{\omega}{u} \right) \mathbf{E}(\mathbf{r}, \omega) + i \frac{\mu_0 \omega^2}{2\beta(\omega)} \mathbf{P}_{nl}(\mathbf{r}, \omega). \quad (15)$$

For a medium with an instantaneous Kerr nonlinearity, the nonlinear polarization, appearing on the right-hand side of Eq. (15), is given by

$$\mathbf{P}_{nl}(\mathbf{r}, \eta) = \varepsilon_0 \chi_3 |\mathbf{E}(\mathbf{r}, \eta)|^2 \mathbf{E}(\mathbf{r}, \eta), \quad (16)$$

where χ_3 is the third-order nonlinear-optical susceptibility and the field $\mathbf{E}(\mathbf{r}, \eta)$ in the time domain is given by the inverse Fourier transform of the field in the frequency domain,

$$\mathbf{E}(\mathbf{r}, \eta) = \text{FT}^{-1}\{\mathbf{E}(\mathbf{r}, \omega)\}. \quad (17)$$

Representing the nonlinear polarization in the form of Eq. (16), we neglect third-harmonic generation and the retarded part of Kerr nonlinearity (i.e., the Raman effect). We thus restrict our analysis here to the case of hollow PCFs filled with non-Raman, e.g., rare, gases.

Multiplying both parts of Eq. (16) by $\mathbf{E}(x, y, \omega)$ and integrating over the transverse coordinates, we reduce Eq. (15) to a one-dimensional equation,

$$\frac{\partial E}{\partial z}(z, \omega) = i \left(\beta(\omega) - \frac{\omega}{u} \right) E(z, \omega) + i \frac{\mu_0 \omega^2}{2\beta(\omega)} P_{nl}(z, \omega), \quad (18)$$

where

$$P_{nl}(z, \omega) = \psi \varepsilon_0 \text{FT}\{|E(z, \eta)|^2 E(z, \eta)\}, \quad (19)$$

$$E(z, \eta) = \text{FT}^{-1}\{E(z, \omega)\}, \quad (20)$$

$$\psi = \frac{\int \int \chi_3(x, y) |E(x, y, \omega)|^4 dx dy}{\int \int |E(x, y, \omega)|^2 dx dy}. \quad (21)$$

The losses are included in Eq. (18) through the imaginary part of the propagation constant β ,

$$\frac{\partial E(z, \omega)}{\partial z} = i\beta_{\text{eff}}(z, \omega)E(z, \omega) - \alpha_{\text{eff}}(z, \omega)E(z, \omega), \quad (22)$$

where

$$\beta_{\text{eff}}(z, \omega) = \beta(\omega) - \frac{\omega}{u} + \frac{\mu_0 \omega^2}{2\beta(\omega)} \text{Re}\left(\frac{P_{\text{nl}}(z, \omega)}{E(z, \omega)}\right), \quad (23)$$

$$\alpha_{\text{eff}}(z, \omega) = \alpha(\omega) + \frac{\mu_0 \omega^2}{2\beta(\omega)} \text{Im}\left(\frac{P_{\text{nl}}(z, \omega)}{E(z, \omega)}\right), \quad (24)$$

with $\alpha(\omega)$ being the intensity-independent magnitude of radiation loss for the waveguide mode.

We solve Eq. (18) using a numerical procedure based on an explicit difference scheme. Simulations were performed for three realistic profiles of dispersion $\beta(\omega)$ and loss $\alpha(\omega)$ [Figs. 1(a)–1(c)], typical of commercial hollow-core PCFs [25]. In what follows, hollow PCFs with dispersion and loss profiles specified in Figs. 1(a)–1(c) will be referred to as PCFs of the first, second, and third type, respectively. Simulations were performed for hollow PCFs filled with a non-Raman gas. Specific values of laser pulse energies and powers will be given for argon-filled hollow PCFs. To make the main conclusions and predictions of the analysis presented below applicable to any other non-Raman gas, characteristic energy parameters should be redefined in such a way as to keep the parameter ψ [Eq. (21)] constant.

With the $\beta(\omega)$ and $\alpha(\omega)$ profiles explicitly included in Eq. (18), our approach does not involve a standard Taylor-series approximation of the dispersion and provides an exact account of waveguide loss. For a better understanding of pulse dynamics in hollow PCFs and especially solitonic phenomena, simulations were also performed with the $\beta(\omega)$ profile approximated with the second; third; and fourth-order polynomial fit. Pulse dynamics calculated with the use of such a model for $\beta(\omega)$ were compared with the results of simulations performed with the exact $\beta(\omega)$ profile. This comparison has visualized effects related to high-order dispersion and allowed the soliton dynamics in a hollow PCF with a realistic dispersion profile $\beta(\omega)$ to be analyzed versus the standard evolution of ideal solitons, defined as solutions to the nonlinear Schrödinger equation (NLSE).

III. RESULTS AND DISCUSSION

A. Soliton dynamics

Our main task in this section is to explore the soliton dynamics of high-power laser pulses propagating through hollow PCFs with dispersion and loss profiles shown in Figs. 1(a)–1(c). We will focus on laser pulses with initial energies of hundreds of nanojoules and initial pulse durations on the order of 100 fs. We will identify propagation regimes when the temporal width of such pulses decreases to tens of femtoseconds. The peak powers will thus typically fall within the megawatt range for the laser fields considered here.

In Fig. 2, we present a typical soliton dynamics of a laser pulse propagating through the first-type PCF. The input pulse energy is set equal to 400 nJ and the initial pulse width is

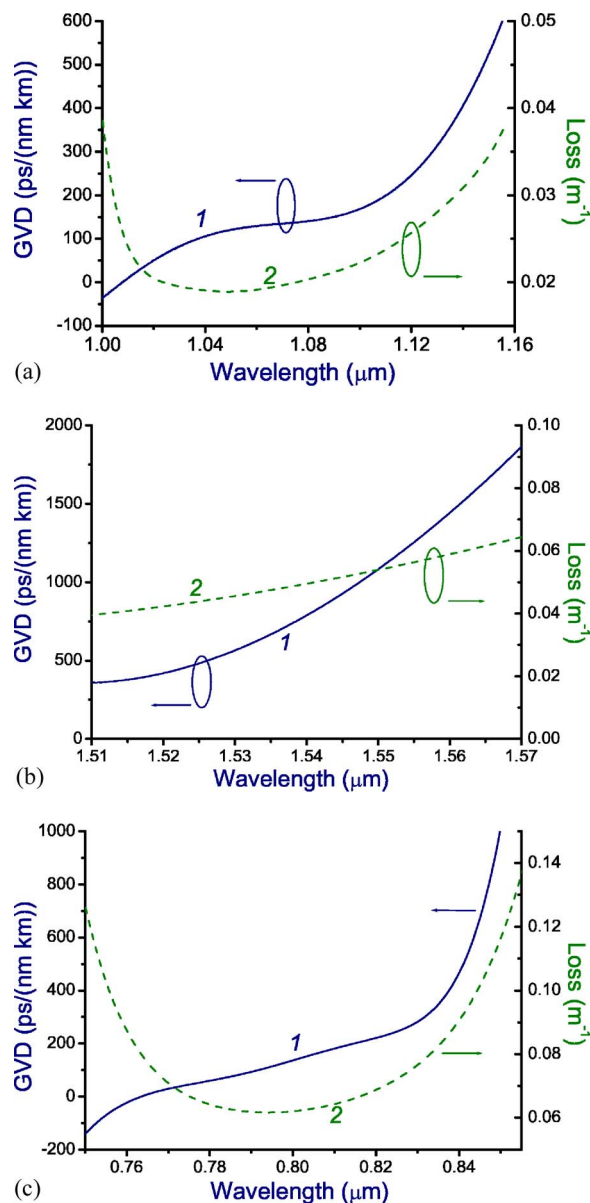


FIG. 1. (Color online) Group-velocity dispersion (solid line 1) and radiation loss (dashed line 2) vs the wavelength for hollow PCFs of the first (a), second (b), and third (c) type.

200 fs (Fig. 2). The central wavelength of the input pulse is $1.08 \mu\text{m}$. Soliton transmission and compression of femtosecond laser pulses with such a central wavelength is of special interest for the development of ytterbium-laser technologies, including all-fiber ytterbium-based oscillator-amplifier systems. The central wavelength of the input field falls within the range of anomalous dispersion of the considered PCF. The input pulse therefore tends to form solitons as it propagates through the fiber, with the pulse shape featuring, at least within the initial section of PCF, a well-pronounced oscillatory behavior (Fig. 2). Such a behavior, as known from the standard NLSE-based theory [26], is typical of high-order solitons. The soliton pulse shape displays one full oscillation cycle within approximately one NLSE soliton period $\Delta z = \pi\tau_0^2(6.2|\beta_2|)^{-1}$, where τ_0 is the initial pulse width defined as the full width at half-maximum and β_2

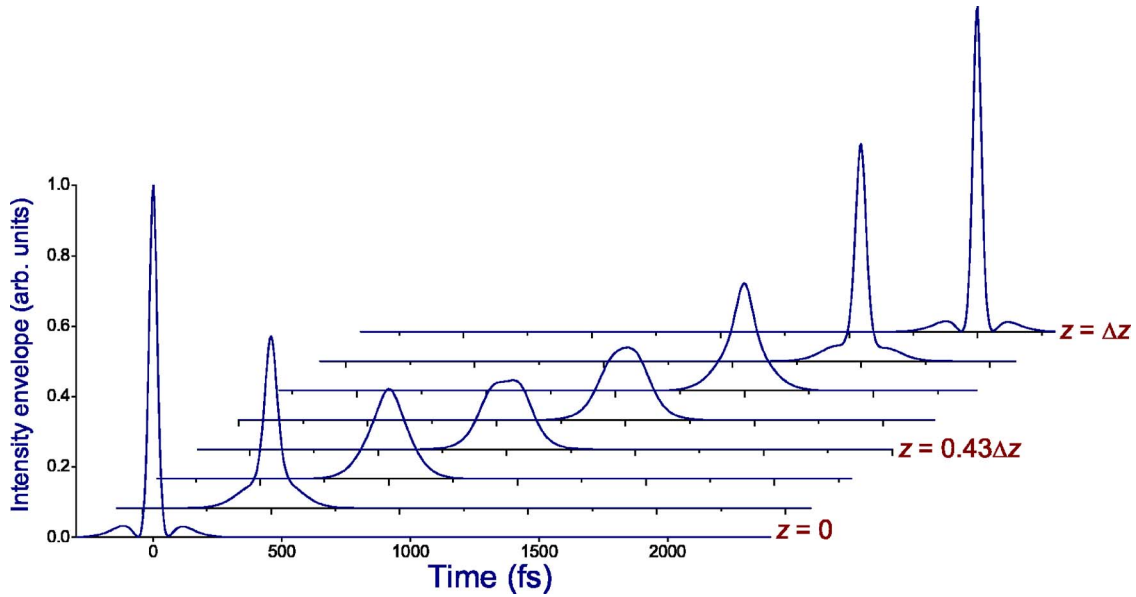


FIG. 2. (Color online) Typical soliton dynamics of a laser pulse propagating through the first-type PCF. The input pulse energy is 400 nJ, the central wavelength of the input pulse is 1.08 μm .

$=\partial^2\beta/\partial\omega^2$ is the parameter characterizing group-velocity dispersion.

Further on along the PCF, deviations from NLSE predictions become noticeable. Physically, these deviations originate from high-order dispersion effects and waveguide losses. To illustrate the evolution of solitons in hollow PCFs, we plot in Figs. 3(a)–3(d) the local soliton pulse width τ as a function of the propagation length z for various input pulse parameters and different types of PCFs. The central wavelengths of input pulses are taken equal to 1.08, 1.53, and 0.8 μm for PCFs of the first, second, and third types, respectively, modeling the soliton transmission of ytterbium, erbium, and Ti:sapphire laser pulses, respectively. As the soliton propagates through a PCF, its energy W [shown by dashed lines in Figs. 3(a)–3(d), corresponding to the right-hand ordinate axis] decreases because of fiber losses. For an NLSE soliton, the temporal full width at half-maximum τ is related to the soliton energy W by the formula [26]

$$W = \frac{\lambda^3 DS}{11.2cn_2\tau}, \quad (25)$$

where λ is the central wavelength of the soliton, $D = -(\lambda/c)d^2n/d\lambda^2$ is the group-velocity dispersion (GVD), $n = \beta/k$ is the effective mode index, n_2 is the nonlinear refractive index of the fiber material, and S is the effective mode area. Based on this insight from the NLSE soliton theory, we can expect that the pulse width of solitons in hollow PCFs should start to increase as the solitons lose their energy propagating through the fiber. This expectation is verified by the results of numerical simulations in Figs. 3(a)–3(c). These results also demonstrate that, as the soliton becomes longer, its oscillation period noticeably increases. This finding is consistent with the NLSE-theory scaling $\Delta z \propto \tau^2$ where the pulse width τ is now understood as a local parameter that changes as a function of the propagation coordinate. In a

fiber with no energy losses [Fig. 3(d)], the oscillatory behavior persists over many meters of pulse propagation length.

For NLSE solitons, the pulse width is related to the pulse energy through Eq. (25). A decrease in the soliton energy W , therefore, results in a lengthening of an NLSE soliton in accordance with the scaling law $\tau \propto W^{-1}$. In hollow PCFs, an additional limitation on the minimum pulse duration originates from the limited transmission band [Figs. 1(a)–1(c)]. With this factor in mind, we transform the NLSE scaling of τ as a function of W into the following ansatz:

$$\tau - \tau_b \propto W^{-1}, \quad (26)$$

where τ_b is the temporal width of a pulse whose spectrum still fits the transmission band of a hollow PCF. Parameters τ and W are now understood as local values of the soliton pulse width and the energy, respectively.

In Fig. 4, we use the ansatz of Eq. (26) to fit the soliton pulse width averaged over the soliton oscillation period as a function of the local soliton energy for high-power solitons propagating through hollow PCFs. Parameters τ_b for hollow PCFs of the first, second, and third types are estimated as $\tau_b \approx \pi/\delta\omega$, where $\delta\omega$ is the spectral width of the fiber transmission band, giving τ_b of about 10, 20, and 10 fs for PCFs of the first, second, and third types, respectively. Numerical simulations, as can be seen from Fig. 4, agree very well with predictions of Eq. (26). This result suggests that, although the dynamics of high-power solitons in hollow PCFs may substantially deviate from the evolution of NLSE solitons, these non-NLSE effects build up adiabatically, so that Eq. (26) holds true for local soliton parameters. In this regime, the average soliton pulse width and the period of oscillatory solitonic dynamics can be estimated from the local value of the soliton energy, decreasing because of fiber losses.

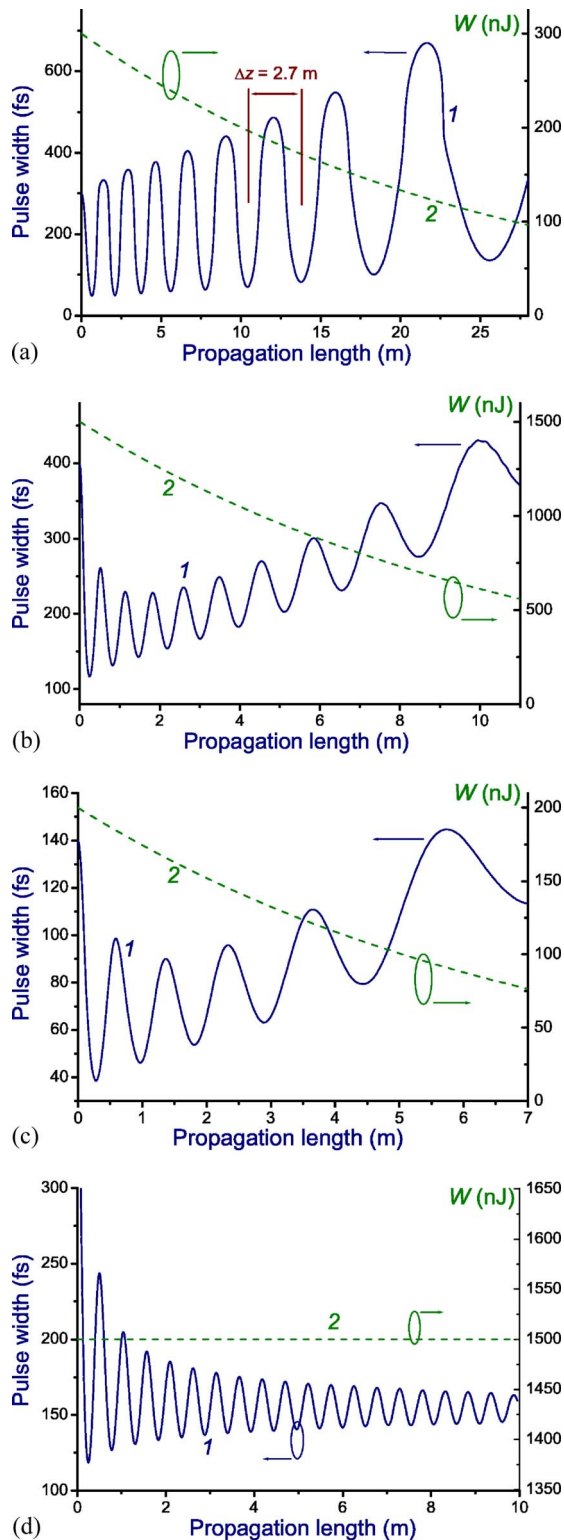


FIG. 3. (Color online) The local soliton pulse width τ (solid line 1) and energy W (dashed line 2) calculated as a function of the pulse propagation length in a hollow PCF of the first (a), second (b), and third (c) type. The central wavelength of the input pulse is $1.08 \mu\text{m}$ (a), $1.53 \mu\text{m}$ (b), and $0.8 \mu\text{m}$ (c). (d) The local soliton pulse width τ (solid line 1) and energy W (dashed line 2) calculated as a function of the pulse propagation length for the second-type hollow PCF with no losses.

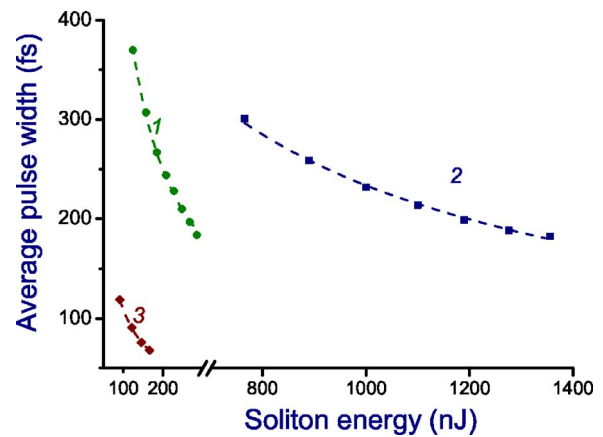


FIG. 4. (Color online) The soliton pulse width averaged over the soliton oscillation period as a function of the soliton energy for high-power solitons propagating through a hollow PCF of the first (1), second (2), and third (3) type. The central wavelength of the input pulse is $1.08 \mu\text{m}$ (1), $1.53 \mu\text{m}$ (2), and $0.8 \mu\text{m}$ (3). The dots, rectangles, and diamonds represent the results of numerical simulations. The dashed lines show the fit of the results of numerical simulations with the use of Eq. (26).

B. Pulse compression

The solitonic dynamics of laser pulses propagating through hollow PCFs suggests attractive strategies for pulse compression. In Figs. 5(a) and 5(b), we illustrate a solitonic evolution of a laser pulse with an initial pulse width of 150 fs and a central wavelength of $1.08 \mu\text{m}$. For an argon-filled hollow PCF with a core diameter of about $10 \mu\text{m}$ [fiber 1, see Fig. 1(a)], the initial energy is set equal to 625 nJ. This energy can, however, be reduced by using gases with higher nonlinearities and/or higher pressures. The input temporal field intensity envelope and the input spectrum are shown by dotted lines 1 in Figs. 5(a) and 5(b), respectively. The dashed and solid lines 2 and 3 in Figs. 5(a) and 5(b) display the temporal field envelopes and pulse spectra at $z=10$ and 16 cm, respectively. At $z=16$ cm, the pulse width, as can be seen from Fig. 5(a), becomes equal to 23.5 fs, which corresponds to a compression ratio of 6.4.

Figures 6(a) and 6(b) display an example of solitonic pulse compression to a pulse width that is close to the limiting pulse duration determined by the transmission band of the fiber. The input pulse in this case has an initial pulse width of 100 fs and a central wavelength of $0.8 \mu\text{m}$ [dotted lines 1 in Figs. 6(a) and 6(b), respectively]. The input pulse energy is set equal to 800 nJ, but it can be reduced by choosing a gas with a higher nonlinearity. The laser pulse propagates through the hollow PCF of the third type with $\tau_b \approx 10$ fs. The minimum pulse width acquired by the pulse with the above-specified parameters is equal to 9.5 fs [Fig. 6(a)], which corresponds to a few-cycle field waveform. The pulse compression ratio for this regime is 10.5.

In Figs. 7(a)–7(c), we present the temporal widths of self-compressing laser pulses with different initial energies calculated as functions of the propagation length for hollow PCFs of three different types with dispersion and loss profiles shown in Figs. 1(a)–1(c). The input pulse energy in these

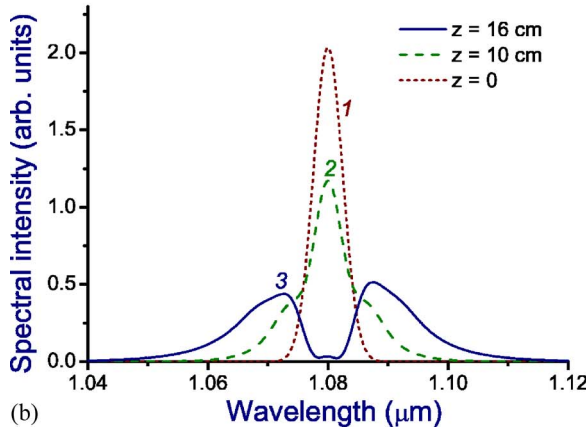
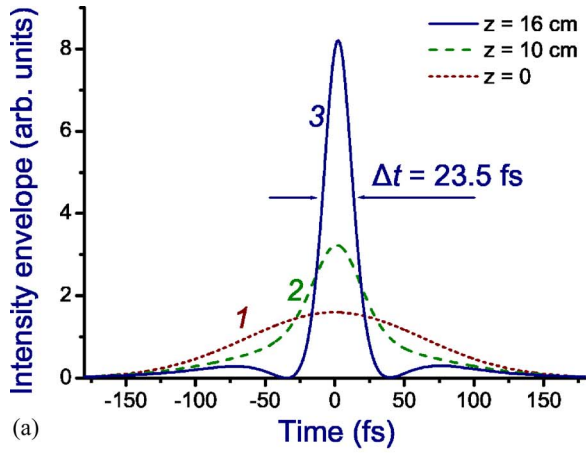


FIG. 5. (Color online) Temporal field intensity envelope (a) and the spectral intensity (b) for a laser pulse with an initial pulse width of 150 fs and a central wavelength of 1.08 μm in the first-type hollow PCF for different propagation lengths: (1) $z=0$, (2) $z=10$ cm, and (3) $z=16$ cm.

simulations ranges from a few to tens of megawatts. The central wavelength of the input laser field was set equal to 1.08, 1.53, and 0.8 μm for PCFs of the first, second, and third types, respectively, allowing us to assess the capabilities of hollow PCFs as compressors for high-power pulses generated by ytterbium, erbium, and Ti:sapphire oscillator-amplifier systems. As can be seen from Figs. 7(a)–7(c), pulses with higher initial energies can be compressed with higher compression ratios. For the first-type hollow PCF, for example, as the input laser energy increases from 300 to 1200 nJ, the minimum pulse width decreases from 48 to 18 fs [Fig. 7(a)]. This tendency, observed also for the other two types of PCFs [Figs. 7(b) and 7(c)], is typical of soliton strategies of pulse compression. The standard empirical design rule for pulse compressors using solitons with a high soliton number $N^2=L_d/L_{nl}=\gamma P_0\tau_0^2/|\beta_2|(L_d=\tau_0^2/|\beta_2|)$ is the second-order dispersion length, L_{nl} is the nonlinear length, and γ is the nonlinear coefficient) is written as [26] $\tau_0/\tau_{\min}\approx 4.1N$. To extend this design rule to the case of moderate N and to include an additional limitation on the pulse width originating from the finite transmission band of hollow PCFs, we represent the minimum temporal width τ_{\min} of a laser pulse in a hollow PCF as a Taylor-series expansion in

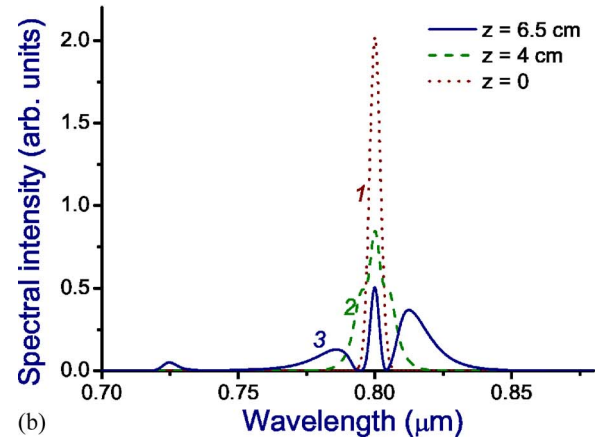
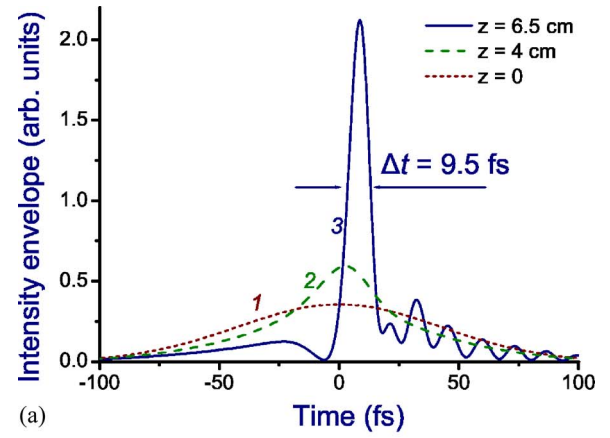


FIG. 6. (Color online) Temporal field intensity envelope (a) and the spectral intensity (b) for a laser pulse with an initial pulse width of 100 fs and a central wavelength of 0.80 μm in the third-type hollow PCF for different propagation lengths: (1) $z=0$, (2) $z=4$ cm, and (3) $z=6.5$ cm.

the small parameter $1/N$ with the zeroth-order term set equal to the minimum pulse width τ_b allowed by the PCF transmission band,

$$\tau_{\min}\approx\tau_b+\tau_0\left(\frac{\xi_1}{N}+\frac{\xi_2}{N^2}+\frac{\xi_3}{N^3}+\dots\right). \quad (27)$$

In view of Eq. (25), Eq. (27) yields the following design rule for a pulse compressor based on a hollow PCF,

$$\tau_{\min}\approx\tau_b+\tau_0\left(\frac{C_1}{W_0^{1/2}}+\frac{C_2}{W_0}+\frac{C_3}{W_0^3}+\dots\right). \quad (28)$$

In Fig. 8, we use Eq. (28) to fit the minimum temporal width of a self-compressing pulse in a hollow PCF as a function of the input energy W_0 for the three above-specified types of fibers. The inclusion of the $W_0^{-1/2}$ term in Eq. (28) was found to be sufficient to accurately fit the $\tau_{\min}(W_0)$ dependence for the first-type PCF (curve 1 in Fig. 8). Terms up to the second order in $N-1$ were necessary to provide a reasonable fit for the $\tau_{\min}(W_0)$ dependence in the case of the second-type PCF (curve 2 in Fig. 8). Curve 3 in Fig. 8 shows

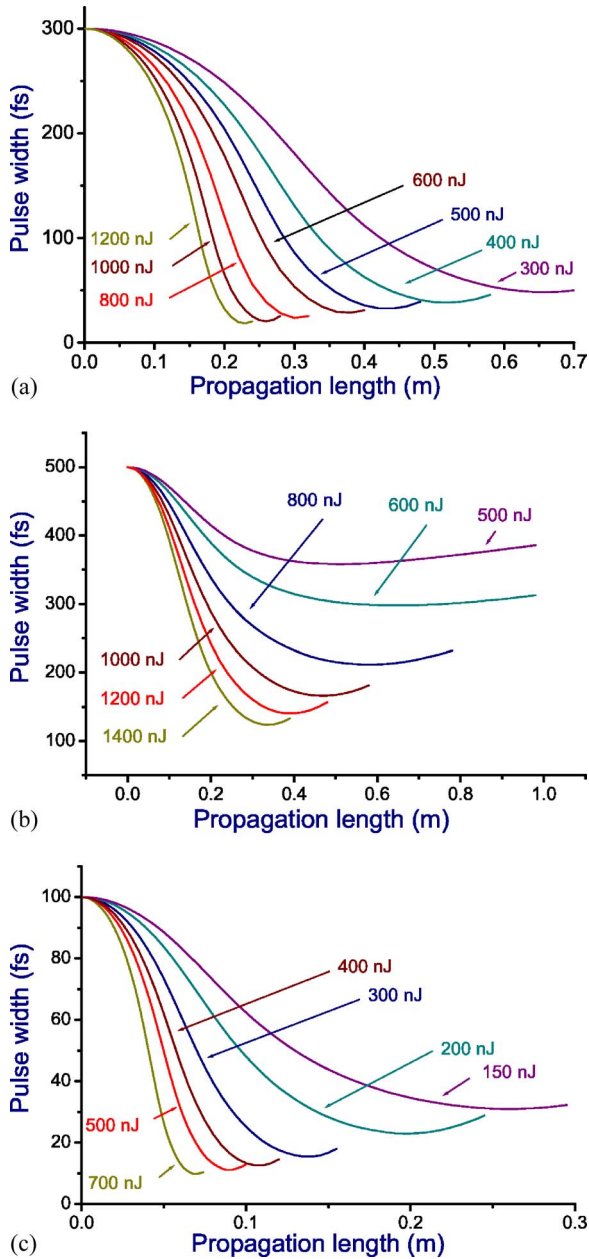


FIG. 7. (Color online) Temporal widths of self-compressing laser pulses with different initial energies (shown in the figures) calculated as functions of the propagation length for hollow PCFs of the first (a), second (b), and third (c) types.

the minimum pulse widths achieved for $0.8\text{-}\mu\text{m}$ laser radiation in the third-type PCF. These data include the dots representing pulse widths shorter than the minimum pulse duration τ_b allowed by the PCF transmission band [see Figs. 6(a) and 6(b)]. In this regime, no reasonable fit for the $\tau_{\min}(W_0)$ dependence was obtained even with $W_0^{-3/2}$ terms included in the expansion of Eq. (28). Excluding these very special cases, the ansatz of Eq. (28) suggests a useful design rule for PCF compressors of high-power laser pulses.

It is interesting and instructive to compare the results of our simulations related to the compression of high-power laser pulses in hollow PCFs with the conclusions of the impressive experimental and numerical work presented by Ou-

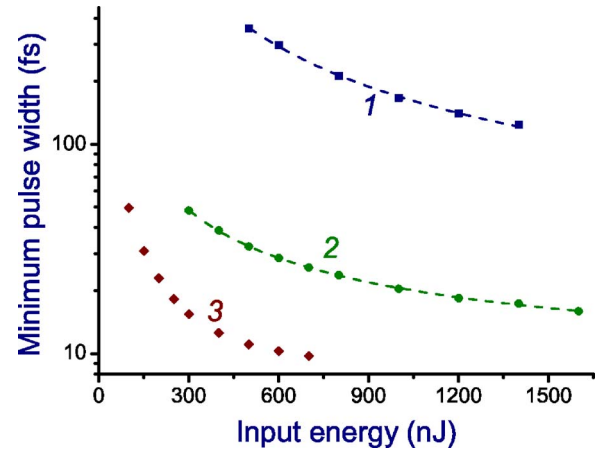


FIG. 8. (Color online) The minimum temporal width of a self-compressing pulse as a function of the input energy W_0 for a hollow PCF of the first (1), second (2), and third (3) type. The central wavelength of the input pulse is $1.08\ \mu\text{m}$ (1), $1.53\ \mu\text{m}$ (2), and $0.8\ \mu\text{m}$ (3). The dots, rectangles, and diamonds represent the results of numerical simulations. The dashed lines show the fit of the results of numerical simulations with the use of Eq. (28).

zounov *et al.* [15], who found that large third-order dispersion limits pulse compression ratios attainable with PCFs used in their experiments to a factor of 2.4. Our simulations confirm the general tendency that high-order dispersion limits pulse compression efficiencies. Moreover, we have shown in the above analysis that further limitations on pulse compression ratios may originate from limited transmission bands of these waveguides, which give rise to frequency-dependent losses, rapidly growing at the edges of PCF transmission bands. To demonstrate high pulse compression ratios in our simulation (6.4 and 10.5 for Figs. 5 and 6, respectively), we minimized, as suggested by Ouzounov *et al.* [15], the influence of high-order dispersion by carefully matching the input central laser wavelength with realistic dispersion profiles of available hollow PCFs. The significance of third-order dispersion effects for laser-pulse evolution can be quantified in terms of the ratio $L_d/L_d^{(3)} = |\beta_3|(|\beta_2|\tau_0)^{-1}$ of the second- to third-order dispersion lengths, with $L_d^{(3)} = \tau_0^3/|\beta_3|$ and $\beta_3 = \partial^3\beta/\partial\omega^3$. For the PCF dispersion profile shown in Fig. 1(a) ($\beta_2 \approx -880\ \text{fs}^2/\text{cm}$ and $\beta_3 \approx 3 \times 10^3\ \text{fs}^3/\text{cm}$) and a pulse width of 100 fs, this ratio is estimated as $L_d/L_d^{(3)} \approx 0.034$ for an input central wavelength of $1.08\ \mu\text{m}$. This estimate has to be compared with the ratio $L_d/L_d^{(3)} \approx 0.28$, which gives the measure of third-order effects for 100-fs pulses propagating in hollow PCFs with $\beta_2 \approx -180\ \text{fs}^2/\text{cm}$ and $\beta_3 \approx 5 \times 10^3\ \text{fs}^3/\text{cm}$, used for pulse compression in experiments by Ouzounov *et al.* [15].

IV. CONCLUSION

We have demonstrated that solitonic regimes of pulse propagation in hollow PCFs allow a control, transmission, and spectral-temporal transformation of ultrashort high-power laser pulses. With the initial parameters of laser radiation accurately matched with fiber dispersion and nonlinear-

ity, submicrojoule laser pulses are shown to exhibit a self-compression and soliton dynamics in the regime of anomalous dispersion. Regimes of solitonic pulse evolution giving rise to few-cycle field waveforms are demonstrated. Based on simple arguments of soliton theory, we derive semiempirical relations providing interesting insights into the minimum pulse width of the laser field in a hollow PCF as a function of the input laser energy. We have demonstrated the potential of specially designed hollow PCFs as pulse compressors, transmission lines, and dispersion-compensation components for ytterbium, erbium, and Ti: sapphire femtosecond laser technologies.

ACKNOWLEDGMENTS

Fruitful discussions with E.E. Serebryannikov are gratefully acknowledged. This study was supported in part by the Russian Foundation for Basic Research (projects 06-02-16880, 04-02-39002-GFEN2004, 03-02-20002-BNTS, and 05-02-90566-NNS), the Russian Federal Research and Technology Program (Contract No. 02.434.11.2010), and INTAS (projects 03-51-5037 and 03-51-5288). The research described in this publication was made possible in part by Award no. RUP2-2695 of the U.S. Civilian Research & Development Foundation for the Independent States of the Former Soviet Union (CRDF).

-
- [1] R. F. Cregan, B. J. Mangan, J. C. Knight, T. A. Birks, P. St. J. Russell, P. J. Roberts, and D. C. Allan, *Science* **285**, 1537 (1999).
- [2] P. St. J. Russell, *Science* **299**, 358 (2003).
- [3] E. A. J. Marcetili and R. A. Schmelzter, *Bell Syst. Tech. J.* **43**, 1783 (1964).
- [4] G. Bouwmans, F. Luan, J. C. Knight, P. St. J. Russell, L. Farr, B. J. Mangan, and H. Sabert, *Opt. Express* **11**, 1613 (2003).
- [5] C. M. Smith, N. Venkataraman, M. T. Gallagher, D. Muller, J. A. West, N. F. Borrelli, D. C. Allan, and K. Koch, *Nature (London)* **424**, 657 (2003).
- [6] S. O. Konorov, A. B. Fedotov, O. A. Kolevatova, V. I. Beloglazov, N. B. Skibina, A. V. Shcherbakov, and A. M. Zheltikov, *JETP Lett.* **76**, 341 (2002).
- [7] A. M. Zheltikov, *Phys. Usp.* **47**, 1205 (2004).
- [8] F. Benabid, J. C. Knight, G. Antonopoulos, and P. St. J. Russell, *Science* **298**, 399 (2002).
- [9] F. Benabid, F. Couny, J. C. Knight, T. A. Birks, and P. St. J. Russell, *Nature (London)* **434**, 488 (2005).
- [10] S. O. Konorov, A. B. Fedotov, and A. M. Zheltikov, *Opt. Lett.* **28**, 1448 (2003).
- [11] A. B. Fedotov, S. O. Konorov, V. P. Mitrokhin, E. E. Serebryannikov, and A. M. Zheltikov, *Phys. Rev. A* **70**, 045802 (2004).
- [12] S. O. Konorov, D. A. Sidorov-Biryukov, A. M. Zheltikov, I. Bugar, D. Chorvat Jr., D. Chorvat, V. I. Beloglazov, N. B. Skibina, M. J. Bloemer, and M. Scalora, *Appl. Phys. Lett.* **85**, 3690 (2004).
- [13] S. O. Konorov, A. M. Zheltikov, Ping Zhou, A. P. Tarasevitch, and D. von der Linde, *Opt. Lett.* **29**, 1521 (2004).
- [14] D. G. Ouzounov, F. R. Ahmad, D. Müller, N. Venkataraman, M. T. Gallagher, M. G. Thomas, J. Silcox, K. W. Koch, and A. L. Gaeta, *Science* **301**, 1702 (2003).
- [15] D. G. Ouzounov, C. J. Hensley, A. L. Gaeta, N. Venkataraman, M. T. Gallagher, and K. W. Koch, *Opt. Express* **13**, 6153 (2005).
- [16] F. Luan, J. C. Knight, P. St. J. Russell, S. Campbell, D. Xiao and D. T. Reid, B. J. Mangan, D. P. Williams, and P. J. Roberts, *Opt. Express* **12**, 835 (2004).
- [17] S. O. Konorov, A. B. Fedotov, O. A. Kolevatova, V. I. Beloglazov, N. B. Skibina, A. V. Shcherbakov, E. Wintner, and A. M. Zheltikov, *J. Phys. D* **36**, 1375 (2003).
- [18] J. D. Shephard, J. D. C. Jones, D. P. Hand, G. Bouwmans, J. C. Knight, P. S. J. Russell, and B. J. Mangan, *Opt. Express* **12**, 717 (2004).
- [19] S. O. Konorov, A. B. Fedotov, V. P. Mitrokhin, V. I. Beloglazov, N. B. Skibina, A. V. Shcherbakov, E. Wintner, M. Scalora, and A. M. Zheltikov, *Appl. Opt.* **43**, 2251 (2004).
- [20] J. Limpert, T. Schreiber, S. Nolte, H. Zellmer, and A. Tünnermann, *Opt. Express* **11**, 3332 (2003).
- [21] C. J. S. de Matos, S. V. Popov, A. B. Rulkov, J. R. Taylor, J. Broeng, T. P. Hansen, and V. P. Gapontsev, *Phys. Rev. Lett.* **93**, 103901 (2004).
- [22] X. Chen, M. Li, N. Venkataraman, M. T. Gallagher, W. A. Wood, A. M. Crowley, J. P. Carberry, L. A. Zenteno, and K. W. Koch, *Opt. Express* **12**, 3888 (2004).
- [23] H. Lim, A. Chong, and F. W. Wise, *Opt. Express* **13**, 3460 (2005).
- [24] A. V. Husakou and J. Herrmann, *J. Opt. Soc. Am. B* **19**, 2171 (2002).
- [25] <http://www.crystal-fibre.com/>
- [26] G. P. Agrawal, *Nonlinear Fiber Optics* (Academic, San Diego, 2001).